Catalytically Active Multicompartment Micelles

Eman Ahmed, Jinwon Cho, Lulu Friedmann, Seung Soon Jang,* and Marcus Weck*

Cite This: *JACS Au* 2022, 2, 2316−2326

Read Online

ACCESS | Metrics & More | Article Recommendations | SI Supporting Information

ABSTRACT: This article presents the self-assembly behavior of multicompartment micelles (MCMs) in water into morphologies with multiple segregated domains and their use as supports for aqueous catalysis. A library of poly(norbornene)-based amphiphilic bottlebrush copolymers containing covalently attached L-proline in the hydrophobic, styrene, and pentafluorostyrene domains and a poly(ethylene glycol)-containing repeat unit as the hydrophilic block have been synthesized using ring-opening metathesis polymerization. Interaction parameter (χ) values between amphiphilic blocks were determined using a Flory−Huggins-based computational model. The morphologies of the MCMs are observed via cryogenic transmission electron microscopy and modeled using dissipative particle dynamic simulations. The catalytic activities of these MCM nanoreactors were systematically investigated using the aldol addition between 4-nitrobenzaldehyde and cyclohexanone in water as a model reaction. MCMs present an ideal environment for catalysis by providing control over water content and enhancing interactions between the catalytic sites and the aldehyde substrate, thereby forming the aldol product in high yields and selectivities that is otherwise not possible under aqueous conditions. Catalyst location, block ratio, and functionality have substantial influences on micelle morphology and, ultimately, catalytic efficiency. "Clover-like" and "core−shell" micelle morphologies displayed the best catalytic activity. Our MCM-based catalytic system expands the application of these nanostructures beyond selective storage of guest molecules and demonstrates the importance of micelle morphology on catalytic activity.

KEYWORDS: multicompartment micelles, amphiphilic bottlebrush copolymer, site isolation, asymmetric aldol addition, micelle morphology, supported catalysis
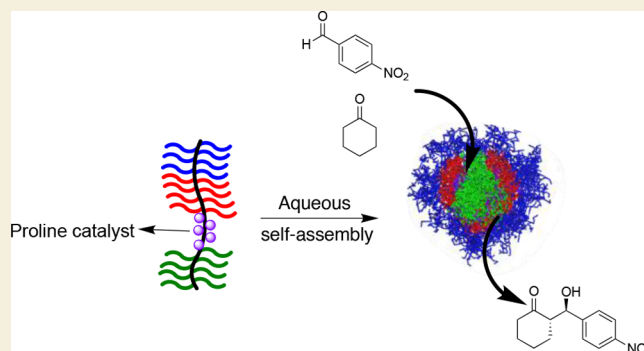
INTRODUCTION

Multicompartment micelles (MCMs), formed from block copolymers, are self-assembled nanostructures that possess multiple discrete domains.[1] MCMs are inspired by biological systems in which a eukaryotic cell, comprising individual compartmentalized subunits, can perform a plethora of distinct functions.[2] Micellar structures formed by traditional hydrophobic−hydrophilic AB diblock copolymers are limited to two distinct domains, that is, the core and the shell.[3] Addition of a third (or more) mutually incompatible polymer block(s) results in the formation of additional spatially separated domains within the nanostructure.[4] Commonly, fluorine-[5−10] or silane-rich[11,12] blocks are used to provide further microphase separation. Polymeric MCMs comprising fluorophilic, siliphilic, lipophilic, and hydrophilic subdomains have been assembled from miktoarm and linear copolymers, and an array of morphologies have been observed, including disk,[13] worm,[7,13] onion,[8,14] flower-like,[15] and patchy nanostructures.[5,14]

MCMs have potential application as the selective storage medium for guest molecules.[13] The presence of a segregated hydrophobic core provides a microenvironment for the encapsulation[16] of these guests and selective release[17,18] of multiple incompatible hydrophobic payloads such as hydrophobic chemotherapeutics,[19,20] nucleic acids,[21] and photosensitizers[22,23] by minimizing the unfavorable interactions between them. The use of functional MCMs for any applications, however, has not been reported. In particular, one can envision to use MCMs for the site isolation of catalytic moieties as a new support system for aqueous catalysis.[24−27] This contribution will close this gap. By covalently attaching the catalyst into the core-forming blocks of the copolymer, MCMs can provide a hydrophobic microenvironment, which is desirable for organic reactions in an overall aqueous medium.

Progress in controlled/living polymerization techniques has led to exceptional control over the dimensions, functionality, and morphologies of MCMs based on block copolymers.[8,11,28]

In particular, bottlebrush copolymers are exceptional building blocks for MCMs. The extended backbone architecture coupled with densely grafted side chains confers bottlebrush copolymers with unique solution assembly behaviors compared to their linear polymer counterparts.[29] Amphiphilic bottlebrush copolymers have a low critical micelle concentration, indicating an enhanced thermodynamic stability, thereby enabling the application of these materials in dilute environments.[30,31] Additionally, the self-assembly behavior of bottlebrush copolymers can be easily manipulated by varying the block ratio and side-chain length to tune complex architectures for applications in technology and therapeutics.[32–38] We have described the self-assembly of bottlebrush copolymers that are prepared by ring-opening metathesis polymerization (ROMP) into MCMs.[11] Herein, we build on these results to expand upon the bottlebrush copolymer-based MCMs into the realm of supported catalysis.

L-Proline has been used widely as a chiral organocatalyst for asymmetric C–C bond formation.[39–44] In the presence of minimal amounts of water, L-proline catalyzes the aldol addition between ketones and aldehydes in high yields and enantiomeric excesses.[45–48] Reactions conducted at a high concentration of water (or just water) exhibit the opposite effect, resulting in low yields and loss of enantioselectivity.[49,50] Clearly, there is great interest in the use of water as a solvent because of its cost effectiveness, high abundance, environmental inertness, and absence of toxicity.[51] Water, however, is often a non-solvent for organic reagents which are commonly hydrophobic.[52–55] Therefore, conducting catalysis in water necessitates the need of a hydrophobic environment within an overall aqueous medium.[56] L-Proline-mediated aldol addition in water has been demonstrated using surfactants[57] and block copolymers[58–61] that shield the catalyst inside the hydrophobic micelle core from the aqueous environment and facilitate the reactivity of organic substrates.

Herein, we report on L-proline (**NB-Proline/NB-Proline-OH**)-functionalized hydrophilic (**H**), lipophilic (**L**), and fluorophilic (**F**) amphiphilic bottlebrush copolymers that assemble into MCMs with adjustable morphologies and exhibit tunability in catalytic activity based on the catalyst location, ratio, and functionality (Figure 1). The amphiphilic bottlebrush copolymers consist of a hydrophobic poly(styrene) and poly(pentafluorostyrene) core surrounded by a solubilizing hydrophilic poly(ethylene glycol) shell. Cryogenic transmission electron microscopy (Cryo-TEM) was used to characterize the MCM morphologies, while dissipative particle dynamic (DPD) simulations were employed to model and predict the self-assembly behavior of the bottlebrush block copolymers. By covalently attaching L-proline to the core-forming block of the bottlebrush block copolymer, the resulting MCMs provide the desired hydrophobic microenvironment for efficient and selective aldol addition in an overall aqueous medium overcoming the water incompatibility of proline-catalyzed aldol additions.

■ RESULTS AND DISCUSSION

Design and Macromonomer Synthesis

There are several design criteria to consider when contemplating the use of MCMs as support for catalysis. First is the nature of the amphiphilic block copolymer. Most block copolymers used in the assemblies of MCMs are synthesized via controlled radical polymerization techniques or undergo tedious post-
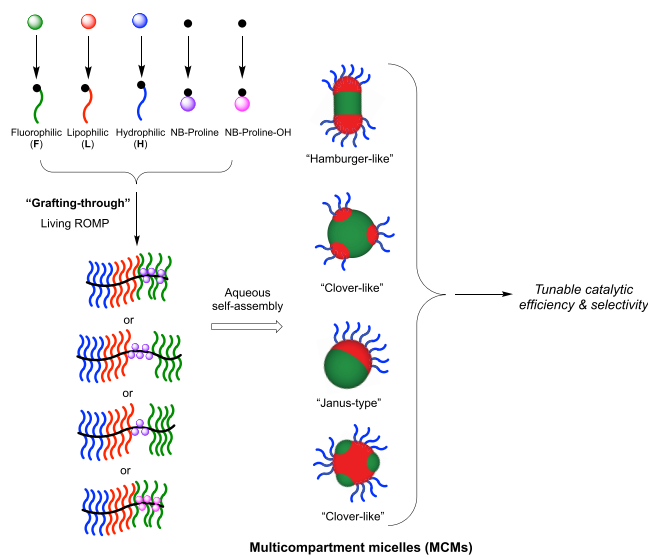

Figure 1. Schematic representation of the strategy toward the synthesis of L-proline-functionalized bottlebrushes that self-assemble in aqueous media into MCMs with unique morphologies and yield tunable catalytic activity. Blue: hydrophilic block (H); red: lipophilic block (L); green: fluorophilic block (F).

polymerization modifications.[7,9,10,62] Other polymerization methods include the use of ROMP to synthesize poly-(norbornene) block copolymers. The living nature of ROMP makes it particularly advantageous for the facile synthesis of amphiphilic block copolymers in one-pot.[8,63] In addition, ROMP offers the benefit of mild reaction conditions and functional group tolerance allowing for the incorporation of chemical handles along the terminal ends, backbone, and side chains of the polymer.[64,65] We use poly(norbornene)s synthesized by ROMP and functionalized with L-proline along the backbone to assemble the MCM catalysts.

The second design criterion is the choice of block sequence and backbone ratio for the bottlebrush copolymers. Modifications to individual block length and block order impact micelle morphology[8] and potentially catalytic performance. To probe the effect of these variables, we synthesized a series of MCMs where the block order and block ratio for the **H**, **L**, and **F** domains (Scheme 1) were held constant, while the block ratio and the position of the L-proline catalyst were varied. For catalysis in water, the diffusion of hydrophobic substrates from the aqueous bulk media into the core is a key factor.[66] The L-proline catalyst was, therefore, either randomly copolymerized with the **F** domain or polymerized as an individual block between the **L** and **F** domains. The ratio for the hydrophilic to hydrophobic domains was based on our prior work where the self-assembly behavior of amphiphilic bottlebrush copolymers was explored and ensured that the volume fraction of each block resulted in stable micelles with distinct compartments.[11]

Lastly, we investigated the effect of catalyst identity on micelle morphology and catalytic activity. We explore two proline derivatives, **NB-Proline** and **NB-Proline-OH**. **NB-Proline** lacks the acidic functionality found in **NB-Proline-OH**, which we hypothesize might impact microphase separation as well as catalysis. Both proline derivatives were functionalized with polymerizable *exo*-norbornenes via amide linkages through the carboxylic acid or ester linkage at the 4-hydroxy position of L-proline, respectively (see Supporting Information).

Scheme 1. Schematic Representation of the Synthesis of Amphiphilic Bottlebrush Copolymers Prepared by ROMP: (a) Triblock Copolymer Formation with the Proline Catalyst Copolymerized in the Fluorophilic Block; (b) Tetrablock Copolymer Formation with the Proline Catalyst Polymerized as an Individual Block between the Lipophilic and Fluorophilic Domains; and (c) Chemical Structures of Monomers H, L, and F and the Protected L-Proline Containing *exo*-Norbornenes
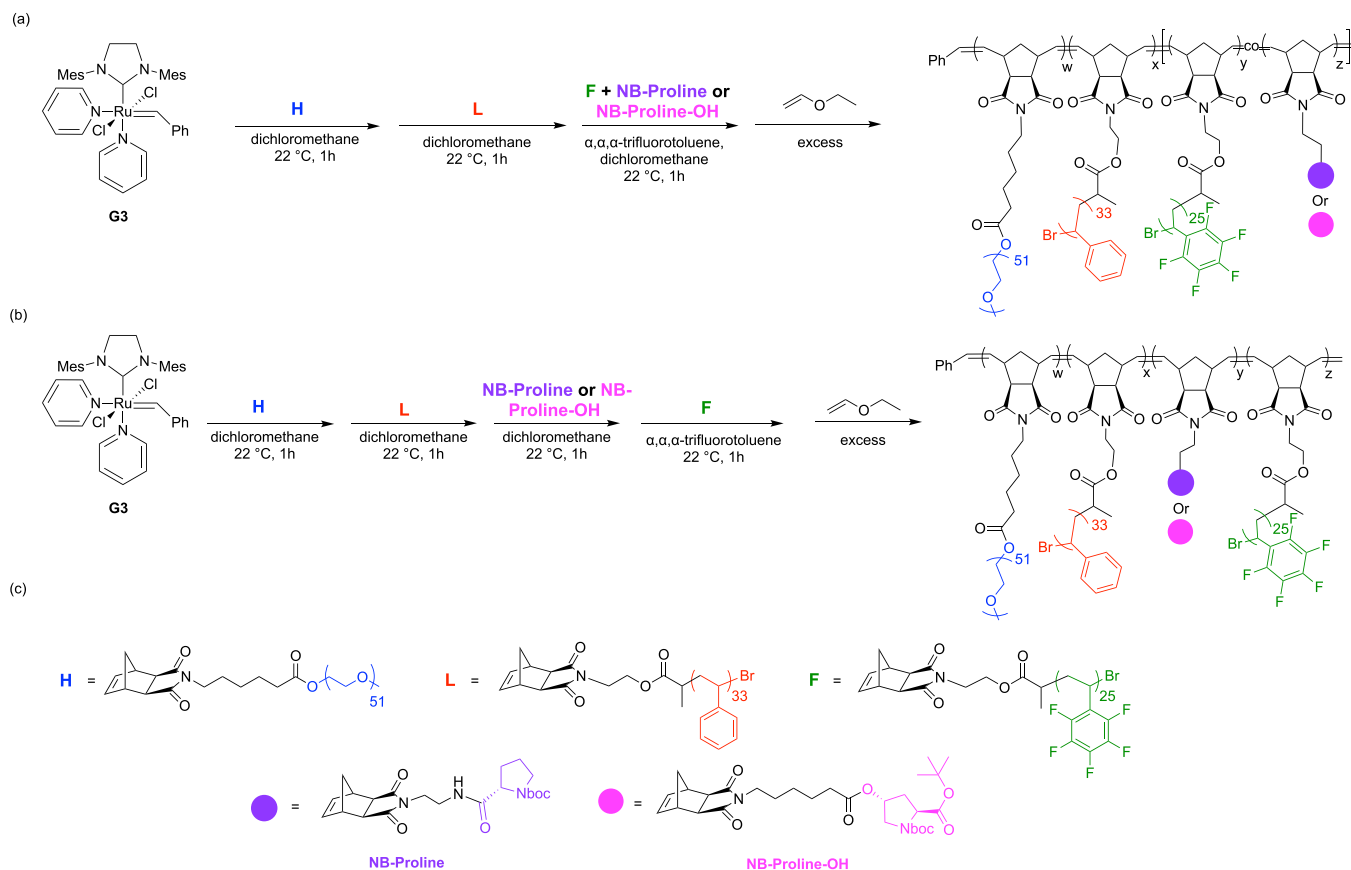

End-functionalized *exo*-norbornene macromonomers **L** and **F** were synthesized via atom transfer radical polymerization (ATRP) using a norbornene-based initiator which allows for the formation of polymers with controlled molecular weights and narrow dispersities.[67] A carboxylic acid *exo*-norbornene was synthesized and attached to commercially available monohydroxy PEG2000 to yield **H**[68] (see Supporting Information for synthesis and characterization details).

Bottlebrush Copolymer Synthesis

To ensure random incorporation of the proline catalyst within the **F** domain, **NB-Proline**/**NB-Proline-OH** was added to the reaction vessel after the addition of **F** (see Methods Section). Prior to the addition of each new macromonomer, completion of the ROMP of the prior macromonomer was confirmed via ^{1}H NMR spectroscopy by observing the shift of the vinyl protons from 6.33 to 5.31−5.80 ppm (Figures S26 and S27).

GPC traces after sequential macromonomer addition displayed complete incorporation of each block and an increase of molecular weight in each step (Figure 2). ROMP kinetics of the macromonomers and catalysts, measured by ^{1}H NMR spectroscopy of a 20:1 monomer to initiator ratio, confirmed complete polymerization of all five blocks within 16 min (Figure S1). Nevertheless, to ensure complete polymerization, we waited an hour between each macromonomer addition. After complete block copolymer formation, the Boc-protecting groups (and the tert-butyl esters in the case of NB-Proline-OH) were hydrolyzed. The disappearance of the tert-
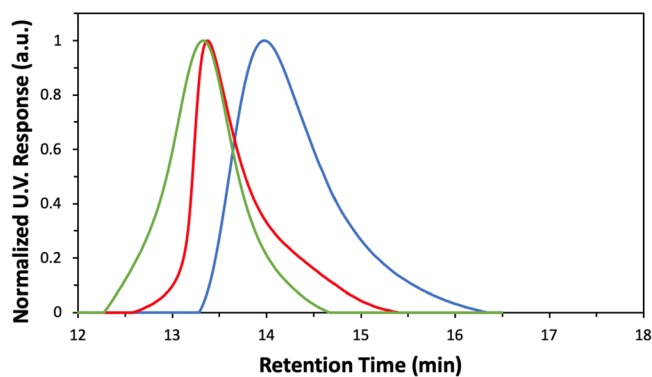

Figure 2. Representative gel-permeation chromatograms for subsequent addition of each block for **P1**. H_{60} in blue; H_{60}−L_{15} in red; H_{60}−L_{15}−[F_{15}−**Proline**$_{36}$] in green. The bottlebrushes were synthesized using Grubbs' third-generation initiator (**G3**) in a one-pot reaction by sequential addition of the macromonomers in dichloromethane (Scheme 1). To improve solubility, a mixed solvent system of α,α,α-trifluorotoluene and dichloromethane was used for the polymerization of **F**.

butyl methyl protons at δ 1.43−1.46 ppm for NB-Proline and δ 1.45−1.47 ppm for NB-Proline-OH in the ^{1}H NMR spectra confirmed complete removal of the protecting group(s) (Figures S206 and 27). The resulting polymers were purified by dialysis against acetone for 3 days.

Table 1. Synthesized Bottlebrush Copolymers with Varying Catalyst Location, Block Ratio, and Functionalities (Proline or Proline-OH)

| polymer | polymer composition | | | | | | GPC characterization | | |
| | % proline/proline-OH | | % S | | % E | | | | |
	theoretical	experimental	theoretical	experimental[c]	theoretical	experimental[d]	Mn_{gpc}[e] (kDa)	Mn_{theor} (kDa)	Đ
P1	$H_{60}-L_{15}-[F_{15}-Proline_{36}]$	28	28[a]	12	16	48	58	58	276	1.48
P2	$H_{60}-L_{15}-Proline_{36}-F_{15}$	28	31[a]	12	12	48	47	45	276	1.22
P3	$H_{60}-L_{15}-Proline_{60}-F_{15}$	40	43[a]	10	13	40	52	49	285	1.15
P4	$H_{60}-L_{15}-Proline_{10}-F_{15}$	10	14[a]	15	16	60	57	89	265	1.38
P5	$H_{60}-L_{15}-[F_{15}-Proline\text{-}OH_{36}]$	28	29[b]	12	13	48	51	81	281	1.19
P6	$H_{60}-L_{15}-Proline\text{-}OH_{36}-F_{15}$	28	22[b]	12	16	48	52	56	281	1.15

[a]Determined via ^1H NMR spectroscopy (CDCl$_3$, 600 MHz) by comparing the integration of the signals of the tert-butyl protons δ (1.43−1.46 ppm) with the signals for the total bottlebrush vinyl protons δ (5.31−5.80 ppm) (see Supporting Information). [b]Determined by comparing the integration of the signals of the tert-butyl protons δ (1.45−1.47 ppm) with the signals of the bottlebrush vinyl protons. [c]Determined by comparing the integration of the signals of the aromatic protons δ (6.40−7.25 ppm) with the signals of the backbone vinyl protons. [d]Determined by comparing the integration of the signals of the methylene protons δ (3.44−3.80 ppm) with the signals of the bottlebrush vinyl protons. [e]THF with 1 vol % triethylamine was used as the eluent for the GPC analyses. Theoretical polymer composition and molecular weights were calculated from the monomer feed ratios.
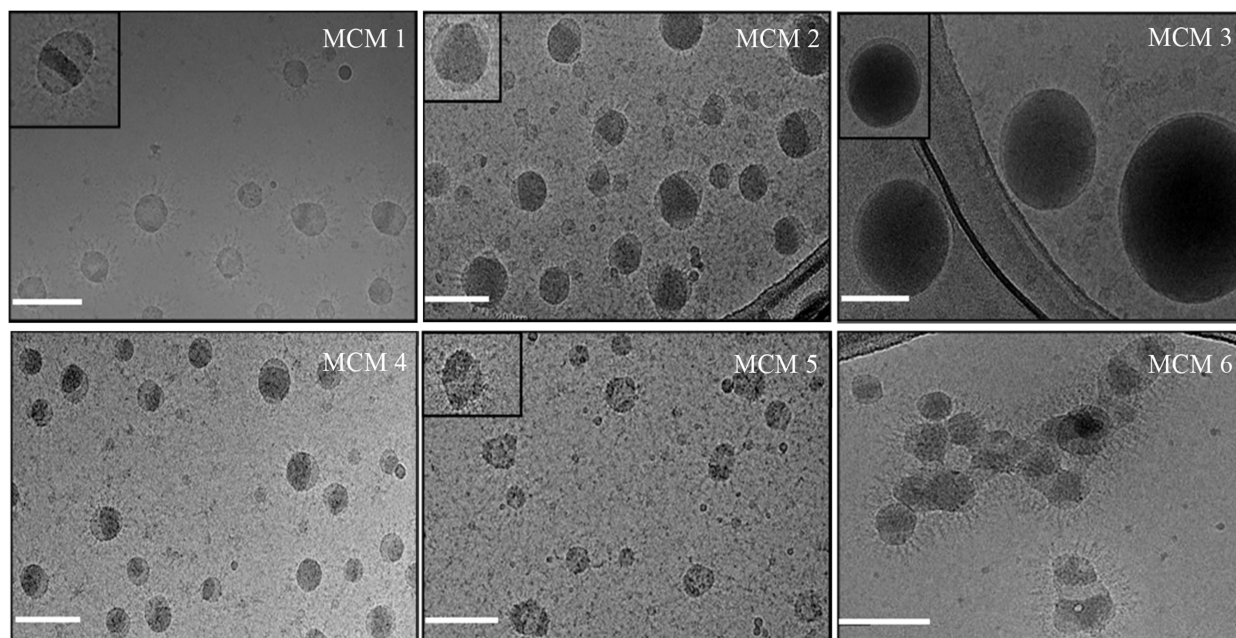
Figure 3. Cyro-TEM images of MCMs 1−6 in water. Scale bars: 100 nm.

Six unique bottlebrush copolymers were synthesized (Table 1). The subscripted values denote the backbone length of each block. The compositions of the bottlebrush copolymers were determined by comparing the integrations corresponding to the poly(styrene) aromatic protons, the PEG methylene protons, and the tert-butyl methyl protons in the ^1H NMR spectra. The percent incorporation of **H**, **L**, and **Proline/Proline-OH** closely matched the feed ratio. The lack of unique proton signals in the ^1H NMR spectrum for **F** limited the accuracy of the final polymer compositions. We were able to confirm the incorporation of **F** via $^{19}F\{^1H\}$ NMR spectroscopy. Gel-permeation chromatography (GPC) traces of **P1−6** displayed monomodal traces with low dispersity (Figure S29). The molecular weights of the polymers determined through GPC analysis, however, were lower than the theoretical value which is in close analogy to the literature where relatively low hydrodynamic radii are observed for bottlebrushes compared to linear polymer analogues.[69]

Micelle Formation and Characterization via Cryo-TEM

Bottlebrush copolymers, **P1−6**, were self-assembled via solvent exchange from tetrahydrofuran (THF) to water to yield functionalized micelles, **MCMs 1−6** at 60 mg mL^{-1} (see Supporting Information). Formation of the MCMs was confirmed by dynamic light scattering analysis (DLS). All DLS traces indicated monomodal size distributions (PDI < 0.7) (Figure S30).[11]

A cryogenic transmission electron microscope was used to image the MCM morphologies of **MCMs 1−6** in water (Figure 3). The images yielded unique morphologies for all six samples highlighting the impact of catalyst location, ratio, and functionality on self-assembly. The nanostructure diameter observed in Cryo-TEM was smaller than those observed via DLS measurements (Figure S30) because of the limited phase contrast of the hydrophilic outer layer in the ice matrix.[12] Microphase separation between the lipophilic and fluorophilic

domains was apparent as the **F** block displays a higher phase contrast due to the increased scattering of the electron beams.

MCM 1, where **NB-Proline** was placed within the **F** domain, formed "hamburger-like"[7] micelles with the fluorophilic region sandwiched between the lipophilic block. **MCM 2**, where **NB-Proline** is placed between the **L** and **F** domains, yielded "clover-like"[70] micelles where the lipophilic domains form the external lobes. By increasing the block ratio of **NB-Proline**, **MCM 3** forms "core−shell" structures, while by decreasing the catalyst ratio, **MCM 4** assembles into "janus-type"[70] particles. **MCM 5**, where **NB-Proline-OH** is placed within the **F** block, results in "clover-like"[70] micelles similar to **MCM 2**; here however, the lipophilic block forms the core, surrounded by the fluorophilic exterior lobes. In **MCM 6**, placing the **NB-Proline-OH** between the **L** and **F** blocks forms "network-like"[7] micelles. To determine the location of the proline catalyst in the nanostructures and confirm the micelle morphology, we obtained interaction parameter (χ) values between each amphiphilic block, followed by DPD simulations.

χ-Parameter Calculations

The Flory−Huggins χ-parameters are required to determine the miscibility between different molecules and consequently their self-assembly behavior. Here, the Flory−Huggins χ-parameter for a pair of polymer blends A and B is defined as eq 1:

$$\chi_{A-B} = \frac{\Delta E_{AB}^{mix}}{RT} \tag{1}$$

where χ_{A-B} and ΔE_{AB}^{mix} indicate χ-parameter and mixing energy between molecules A and B, respectively. In the previous study,[71,72] we established a computational procedure to evaluate the χ-parameter consistently and precisely by using the enhanced ΔE_{AB}^{mix} calculation via implementation of coordination number of B surrounding A (Z_{AB}), the volume enclosed by the solvent-excluded molecular surface over a pair of molecules A and B (V_{AB}), the number of monomeric units (n), reference volume (V_{ref}), and interaction energy between molecules A and B (E_{AB}^*), respectively,

as described in eq 2:

$$\Delta E_{AB}^{mix} = \frac{V_{ref}}{2n} \left[\frac{E_{AB}^*}{V_{AB}} \left(\frac{Z_{AB}}{n_A} + \frac{Z_{BA}}{n_B} \right) \right.$$
$$\left. - \left(\frac{E_{AA}^*}{V_{AA}} \frac{Z_{AA}}{n_A} + \frac{E_{BB}^*}{V_{BB}} \frac{Z_{BB}}{n_B} \right) \right] \tag{2}$$

Since the ΔE_{AB}^{mix} in eq 2 utilizes more physical and chemical properties than the original form of mixing energy, $\Delta E_{AB}^{mix} = E_{AB}^* - \frac{1}{2}(E_{AA}^* + E_{BB}^*)$, the accuracy of χ-parameter results has improved and showed good agreement with the experimental measurements for numerous cases.[71]

As summarized in Table 2, we found that, among the amphiphilic blocks, **F**-water pair demonstrates the highest χ-parameter ($\chi_{F-Water} = 0.963$), followed by **L**-water ($\chi_{s-Water} = 0.756$), **NB-Proline**-water ($\chi_{proline-Water} = 0.459$), and **H**-water pair ($\chi_{E-Water} = 0.197$), implying that blocks **F** and **H** are predicted to be the most hydrophobic and hydrophilic, respectively. Amphiphilic bottlebrush block copolymers **H**, **L**, **F**, and **NB-proline**/**NB-proline-OH**, self-assembled in water, are expected to comprise hydrophilic block **H** in the outermost shell, which is directly in contact with water molecules. In the

**Table 2. Calculated χ-Parameter Values for Each Molecular Pair**

χ_{A-B}	L	H	F	NB-Proline	NB-Proline-OH	Water
L		1.461	0.945	1.075	1.244	0.756
H			0.735	0.531	0.286	0.197
F				1.220	1.449	0.963
NB-Proline						0.459
NB-Proline-OH						0.318

same manner, blocks **L** and **F** would be most likely forming the core of the micelle owing to their hydrophobic nature. Considering that the **H−L** pair shows the highest χ-parameter ($\chi_{H-L} = 1.461$) among polymer−polymer interactions, blocks **H** and **L** are found to be immiscible, and they are likely to undergo a distinct phase separation within the micelle. Likewise, blocks **L** and **F** are highly prone to phase separation within the core of the micelle due to their relatively high χ_{L-F} value of 0.945, which is also observed in the experimental Cryo-TEM images of **MCMs 1−6** displayed in Figure 3. Both **NB-proline** and **NB-proline-OH** catalysts are less hydrophilic than block **H** as χ-parameters are higher for proline-water and proline-OH-water pairs and lower for block **H**. At the same time, they are not readily miscible with blocks **H** and **F**, indicating that the proline catalysts may be sandwiched between the core and shell region.

Micelle Characterization via DPD Simulations

We conducted DPD simulations to predict the micelle morphologies for **MCMs 1−6** based on the χ-parameters in Table 2. Overall, the computed micelle morphologies (Figure 4) are in good agreement with the Cryo-TEM images. We observe a distinct phase separation in the core region between blocks **L** and **F** in MCMs, which is confirmed by the large χ_{L-F} value (0.945). The cross-sectional image of **MCM 1** shows that the **F** domain is formed in the middle of the core and sandwiched between the block **S** domains. **MCMs 2** and **3** yield a "clover-like" and "core−shell" morphology, respectively, as block **S** covers the fluorophilic **F** domains. The increased proline catalyst contents for **MCM 3** promote a more defined fluorophilic core than for **MCM 2**. When the proline content is significantly decreased to a 10-mer for **MCM 4**, unlike **MCM 2**, the block **L** domain is sandwiched between block **F**. For **MCM 5**, **Proline-OH** triggers the formation of a "clover-like" particle where the **F** block surrounds the **L** domain. A ring-shaped block **L** encapsulates the **F** domain for **MCM 6**.

To further quantitatively characterize the intermolecular structure of **MCMs 1−6**, the pair correlation function $[p_i g(r)]$ analysis of the proline catalyst and each domain was evaluated, where $p_i g(r)$ is defined as
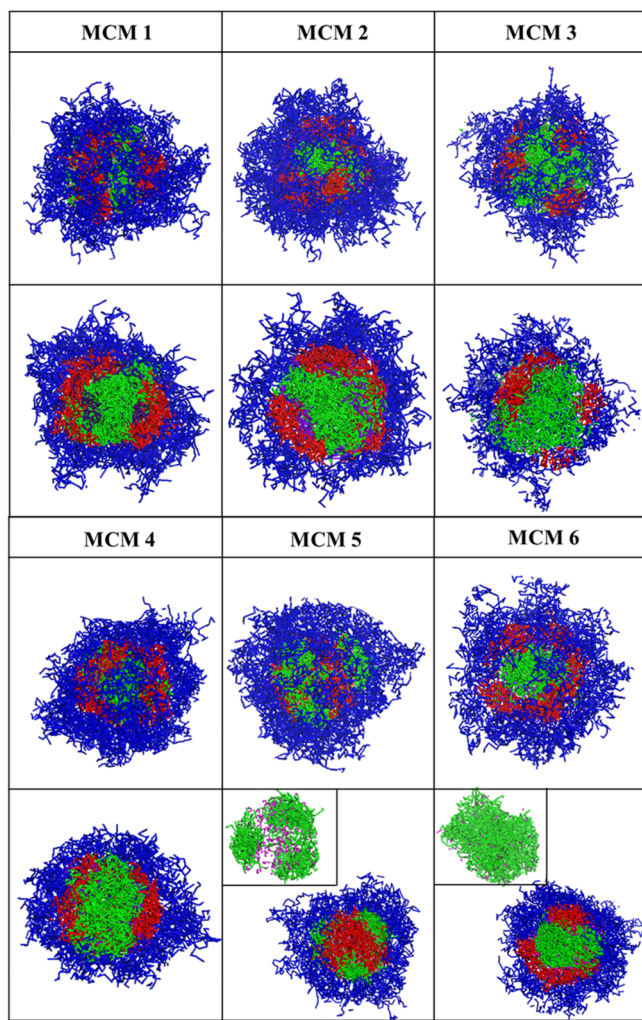
Figure 4. DPD simulation results for **MCMs 1−6**. Top and bottom row represents micelle morphologies and cross-sectional images, respectively. Water molecules are selectively excluded for a clear view of polymers and micelles. **H**, **L**, and **F** blocks are represented in blue, red, and green, respectively. **Proline** and **Proline-OH** beads are represented in purple and pink, respectively. For **MCMs 5−6**, the insets are provided to illustrate the location of proline. Here, **H** and **L** are intentionally excluded for better visualization.

$$p_i g(r) = \frac{n_{\text{proline(proline-OH)}-i}}{4\pi r^2 \Delta r} \tag{3}$$

where p_i denotes the number density of i (block **H**, **L**, or **F**) and r and Δr are the distance between **proline**/**proline-(OH)** and block bead and the shell thickness, respectively. Figure 5 shows that the **Proline−L** pair exhibits a stronger first peak intensity of $g(r) = 31.81$ and $g(r) = 42.80$ for **MCMs 2** and **3**, respectively, than the **Proline−F** pair, indicating that the number of **Proline** catalyst distribution around block **L** is higher than around block **F**. The opposite is true for **MCMs 1**, **4**, **5**, and **6**. Considering that increasing the block ratio of **NB-Proline** more than 36-mer within MCMs does not affect the conversion rate, the location of **NB-Proline** instead plays a critical role in boosting the catalytic activities.

Micelle-Supported Aldol Addition

To investigate the impact of micelle morphologies on catalyst activity, the asymmetric aldol addition between 4-nitro-benzaldehyde and cyclohexanone was used as the model
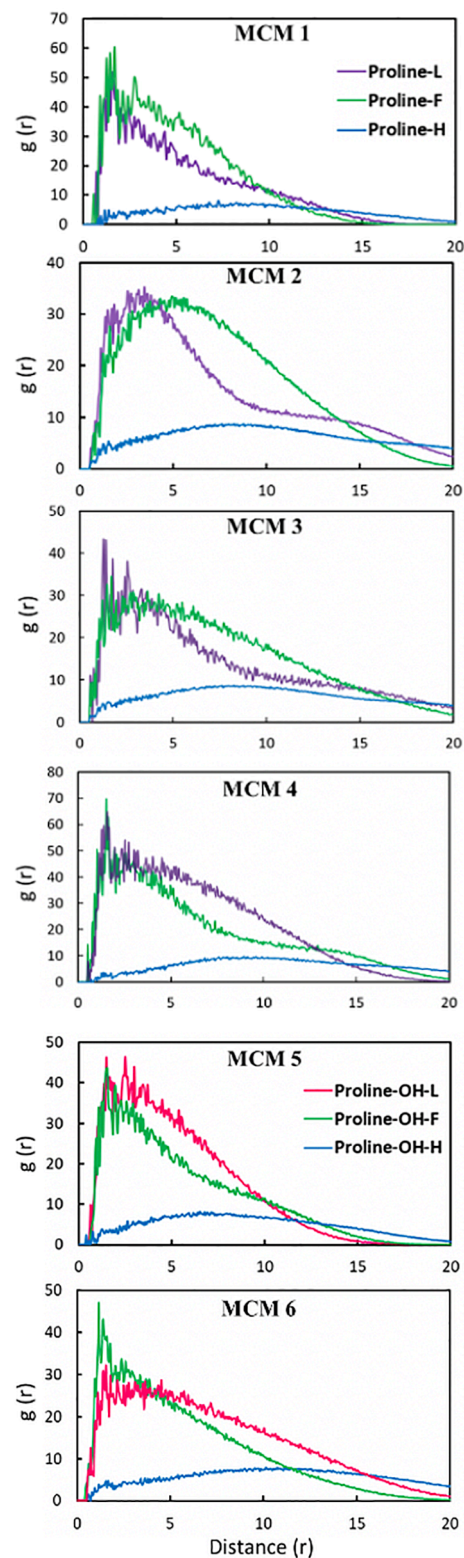

Figure 5. Pair correlation function analysis for the pairs of proline (**MCMs 1−4**)/proline-OH (**MCMs 5−6**) with blocks **H**, **L**, and **F** in **MCMs 1−6**, represented in purple/pink, red, and green lines, respectively.

reaction. Compared with unsupported L-proline-catalyzed aldol addition in water where no reaction is observed due to insolubility of substrates,[59] **MCMs 1−6** demonstrated catalytic

activity in aqueous environments with outstanding enantiose-lectivities (Table 3).

Table 3. Activity and Selectivity of the Functionalized MCMs Corresponding to Polymers P1−P6 for the Aldol Addition in Water[a]
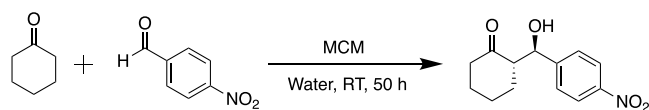
MCM	conversion (%)[b]	anti/syn (%)[b]	ee (%)[c]
1	43	93/7	92
2	95	89/11	92
3	94	88/12	93
4	69	85/15	91
5	37	76/24	89
6	60	82/18	92

[a]Reaction conditions: all reactions were performed with cyclohexanone (7 equiv); [S] = 0.28 M; 20 mol % catalyst loading in water at room temperature for 50 h. [b]Determined by ^{1}H NMR spectroscopy. [c]Determined by chiral HPLC (OD-H, 254 nm, hexane/IPA 9/1, 0.4 mL min^{-1}).

The location of the organocatalysts is key for conversions and selectivities. When **NB-Proline/NB-Proline-OH** is randomly polymerized within the **F** domain (Table 3, **MCMs 1** and **5**), final conversions after 50 h are significantly lower, 43 and 37%, respectively, in comparison to the incorporation of the proline as an individual block between the **L** and **F** domains, which yielded 95 and 60% conversions (Table 3, **MCMs 2** and **6**). MCMs functionalized with **NB-Proline-OH** (**MCMs 5** and **6**) display lower reactivities (37 and 60%) in comparison to those with **NB-Proline** (**MCMs 1** and **2**). This difference can be accounted for by the catalyst functionality, as indicated by the χ-parameter values (Table 2) that leads to unique microphase separation within the micelle nanostructures. Increasing the block ratio of **NB-Proline** from a 36-mer (**MCM 2**) to a 60-mer (**MCM 3**) does not impact conversions (95 and 94%, respectively). Decreasing the block ratio from a 36-mer to a 10-mer, however, reduces the efficiency of the nanoreactor from 95 to 69%.

Figure 6 displays the kinetics data of the reaction catalyzed by **MCMs 1−6** over 50 h. **MCMs 2** and **3** that are **NB-Proline**-functionalized display similar kinetics. **MCMs 1** and **4**, however, display lower reactivities. **NB-Proline-OH**-functionalized MCMs (Figure 4b) display nearly identical conversions during the first 10 h, after which **MCM 6** exhibits higher reactivity reaching 60% within 50 h.

The observed reactivity trends can be accounted for by the micelle morphology. We hypothesize that the faster reaction kinetics of **MCM 2** compared to that of **MCM 1** are due to easier access to the catalytic sites. As confirmed by the pair correlation functions (Figure 5), in **MCM 2**, **NB-Proline** is in closer proximity to the **S** block that forms the exterior lobes of the "clover-like" micelles, contrary to **MCM 1**, where the catalytic site is sandwiched between the lipophilic domains of the "hamburger-like" micelles. **MCMs 2** and **3**, which yield "clover-like" and "core−shell" micelles, respectively, have higher kinetic activity compared to **MCM 4**, possibly due to a larger exposure of the lipophilic surface area to the aqueous environment resulting in a greater number of collisions between substrates and the active site. The low reactivity of
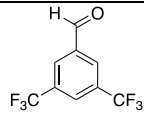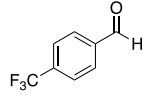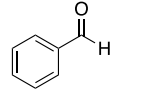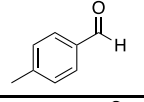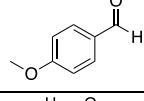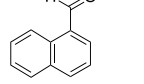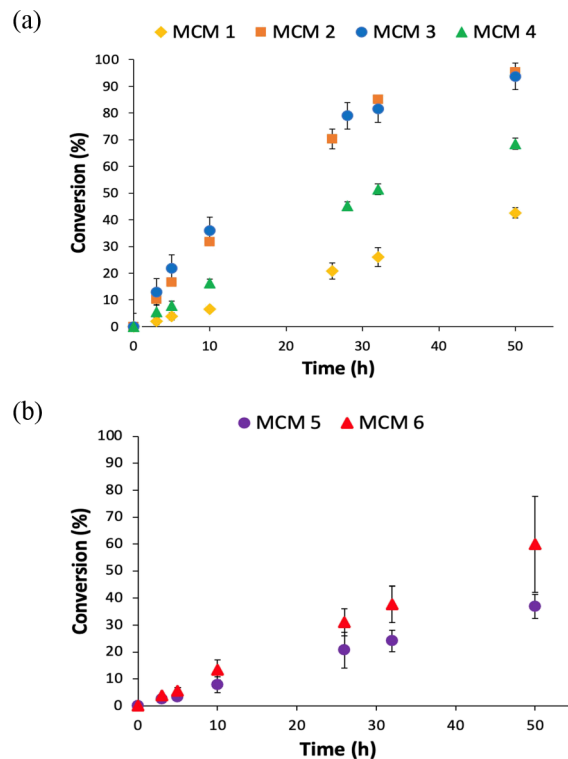

Figure 6. Conversions vs time for the aldol addition between 4-nitrobenzaldehyde and cyclohexanone catalyzed by (a) **MCMs 1−4** (**NB-Proline**-functionalized) and (b) **MCMs 5** and **6** (**NB-Proline-OH**-functionalized). All reactions were performed at 20 mol % catalyst loading; 7 equiv of cyclohexanone; [S] = 0.28 M and at room temperature.

MCM 5 compared to that of all other samples can be explained by the position of the superhydrophobic fluorophilic lobes ($\chi_{F\text{-water}}$ = 0.963, Table 2), which potentially limits the diffusion of water for efficient aldol addition. In **MCM 6**, we hypothesize that the "network-like" micelles hinder access of substrates to the active sites, thereby reducing its activity when compared to that in **MCMs 1−4**.

We performed catalytic control experiments on unfunctionalized micelles assembled from the bottlebrush copolymer, $H_{60}−L_{15}−F_{15}$. In the absence of a catalyst-functionalized micelle core, no reaction was observed under the conditions used for MCM-supported catalysis, confirming the inertness of the bottlebrush copolymer (Table S1, entry a). Additionally, no catalytic transformation was observed when adding the small molecule L-proline to the unfunctionalized micelle solution (Table S1, entry b). This demonstrates the need to compartmentalize the catalyst inside the micellar core for the catalysis of hydrophobic substrates in water.

A substrate screen was performed using **MCM 2** (Table 4). The reaction between cyclohexanone and six aromatic aldehydes was investigated. Aldehydes substituted with electron-withdrawing groups (entries 1 and 2) offered the corresponding aldol products in high yields and selectivities. Benzaldehyde (entry 3) resulted in low conversion, while aldehydes substituted with electron-donating groups (entries 4, 5, and 6) displayed no reaction. We attribute this observation to the decreased electrophilicity at the aldehyde carbon in the absence of electron-withdrawing groups, resulting in low/no reactivity.[73]

Table 4. Substrate Scope for the Aldol Addition of Aromatic Aldehydes with Cyclohexanone Using MCM 2

Entry[a]	Substrate	Conversion (%)[b]	anti/syn (%)[b]	ee (%)[c]
1	(3,5-bis(trifluoromethyl)benzaldehyde)	78	93/7	93
2	(4-(trifluoromethyl)benzaldehyde)	50	91/9	92
3	(benzaldehyde)	7	86/14	N.D.
4	(4-methylbenzaldehyde)	0	N.D.	N.D.
5	(4-methoxybenzaldehyde)	0	N.D.	N.D.
6	(1-naphthaldehyde)	0	N.D.	N.D.

[a]Reaction conditions: all reactions were performed with cyclohexanone (7 equiv); [S] = 0.28 M; 20 mol % catalyst loading in water at room temperature for 50 h. [b]Determined by ^{1}H NMR spectroscopy. [c]Determined by chiral HPLC (OD-H, 210 nm, hexane/IPA 9/1, 0.4 mL min^{-1}). N.D. = not determined.

CONCLUSIONS

This article describes the synthesis and aqueous self-assembly of the first catalytically active MCMs using amphiphilic bottlebrush copolymers. These copolymers are featured with a PEG-based hydrophilic block, a styrene-rich lipophilic domain, a pentafluorostyrene fluorophilic block, and a proline-functionalized catalytic core. Six MCMs with varying catalyst location, backbone length, and/or proline functionality were assembled and tested for the aldol addition between 4-nitrobenzaldehyde and cyclohexanone in water. The MCMs demonstrated catalytic activity in an aqueous environment with full control over yields and enantioselectivities that is otherwise not possible. Systematic investigations demonstrated that the polymer composition and catalyst location had a significant impact on the assembled nanostructures and consequently the catalytic efficiency. The more hydrophobic, **NB-Proline** catalyst demonstrated a higher activity compared to that of **NB-Proline-OH** due to minimal diffusion of water and efficient diffusion of substrates. Polymerizing the catalyst as an individual block rather than copolymerizing it within the **F** domain yielded the best catalytic activity due to easy access to the active sites. Cryo-TEM and DPD simulations were used to characterize the self-assembly behavior of the micelles.

Our work displays an understanding of the impact of micelle morphology on its catalytic applications, which is of utmost importance when expanding the use of these systems for multistep catalysis. While the simplest core−shell nanoparticle can accommodate a catalyst in the core and the shell, MCMs offer a large variety of possibilities to store multiple catalysts in compartments.[8,11] The monomers to synthesize polymeric MCMs can be varied easily, resulting in full control over shape, size, and compartment distribution, which allows for tuning of the catalytic processes. Additionally, compartment sizes are typically in the range of 10−50 nm[24] minimizing the diffusion path from the catalytic center to the center and providing the spatial proximity needed for cascade transformations. With an ongoing focus on exploring the design of polymeric particles for nonorthogonal cascade reactions, future research in our group will leverage the use of MCMs for multistep incompatible transformations.

METHODS

ROMP Polymerization

Formation of the bottlebrush copolymer was conducted in a glovebox under a N$_2$ atmosphere. A 10 mg/mL stock solution of G3 in dry dichloromethane was prepared in a 20 mL scintillation vial. Stock solutions for **H**, **L**, **NB-Proline**, and **NB-Proline-OH** were prepared by dissolving the determined amount of monomer in dry DCM to achieve a final concentration of 0.02 M. A stock solution of **F** was prepared by dissolving the determined amount of monomer in dry, distilled α,α,α-trifluorotoluene to achieve a final concentration of 0.05 M. The amount of each monomer/ macromonomer chosen was based on the targeted backbone degree of polymerization. To initiate the reaction, the monomer solution was added into the catalyst solution and then stirred vigorously at 22 °C. Each subsequent addition was carried out after 1 h to ensure complete polymerization of each block that was monitored by ^{1}H NMR spectroscopy. To ensure that the catalyst monomers were randomly polymerized within the **F** block, the **F** macromonomer was first added, followed by the addition of **NB-Proline**/**NB-Proline-OH**. Ethyl vinyl ether was added to terminate the polymerization, and the reaction mixture was stirred for another 15 min. The solvent was removed by rotary evaporation, and the crude polymer was purified by dialysis in a 10 kDa bag against acetone overnight.

Boc Group and Tert-Butyl Ester Hydrolysis

Polymer samples containing Proline were dissolved in 2 mL of CHCl$_3$/TFA 1/1, and samples containing Proline-OH were dissolved in 2 mL of CH$_2$Cl$_2$/TFA 1/1. The mixture was stirred at room temperature for 24 h. Afterward, the volatiles were evaporated, and the polymer was re-dissolved in acetone and dialyzed in a 2 kDa bag for 3 days. The polymer was recovered as a light brown powder after rotary evaporation.

Micelle Formation

In a vial, the desired amount of the block copolymer (20 mol % catalyst loading) was dissolved in 1.5 mL of THF and stirred at room temperature. Complete polymerization of each block was assumed, and the amount of the polymer sample was calculated using the theoretical molecular weight. Once the polymer was dissolved, 0.5 mL of deionized water was added to the solution and stirred for 15 min with the vial cap on. Afterward, the mixture was stirred overnight uncovered to allow the THF to evaporate, thereby forming micelles. The cap was placed on the vial once all the THF evaporated, and micelle formation was confirmed via DLS.

Proline-Supported Aldol Addition

4-Nitrobenzaldehyde (3 mg, 0.02 mmol, 1 equiv, [0.28 M]) and cyclohexanone (14 μL, 0.14 mmol, 7 equiv) were added to the micelle solution (amount adjusted for 20% catalyst loading). For the substrate screen, the substrate concentration of the aromatic aldehydes was maintained at 0.28 M. The micelle solution was shaken and vortexed to give a homogeneous solution. 20 μL aliquot of the reaction was removed at regular intervals and added to 0.75 mL of CDCl$_3$. The substrates/products were extracted and filtered through a small layer of Na$_2$SO$_4$. The percent conversion was determined by comparison of the 4-nzitrobenzaldehyde aromatic peak at 8.40 ppm to the aromatic

peak of the aldol product peak at 8.20 ppm. The enantiomeric excess was determined by chiral HPLC chromatography.

Additional details for the synthesis and characterization of small molecules and macromonomers, micelle characterization, and computation are included in the Supporting Information.

ASSOCIATED CONTENT

Supporting Information

The Supporting Information is available free of charge at https://pubs.acs.org/doi/10.1021/jacsau.2c00367.

Materials, synthetic procedures, and characterization of small molecules and macromolecules (PDF)

AUTHOR INFORMATION

Corresponding Authors

Seung Soon Jang − *School of Materials Science and Engineering, Georgia Institute of Technology, Atlanta, Georgia 30332-0245, United States*; Email: seungsoon.jang@mse.gatech.edu

Marcus Weck − *Molecular Design Institute and Department of Chemistry, New York University, New York, New York 10003, United States*; orcid.org/0000-0002-6486-4268; Email: marcus.weck@nyu.edu

Authors

Eman Ahmed − *Molecular Design Institute and Department of Chemistry, New York University, New York, New York 10003, United States*

Jinwon Cho − *School of Materials Science and Engineering, Georgia Institute of Technology, Atlanta, Georgia 30332-0245, United States*

Lulu Friedmann − *Molecular Design Institute and Department of Chemistry, New York University, New York, New York 10003, United States*

Complete contact information is available at:
https://pubs.acs.org/10.1021/jacsau.2c00367

Author Contributions

E.A. and J.C. contributed equally as the first authors. CRediT: **Eman Ahmed** conceptualization, data curation, formal analysis, investigation, methodology, writing-original draft, writing-review & editing; **Jinwon Cho** formal analysis, investigation, validation, writing-review & editing; **Lulu Friedmann** investigation; **Seung Soon Jang** funding acquisition, project administration, supervision, writing-review & editing; **Marcus Weck** conceptualization, funding acquisition, project administration, supervision, writing-original draft, writing-review & editing.

Notes

The authors declare no competing financial interest.

ACKNOWLEDGMENTS

REFERENCES

(1) Laschewsky, A. Polymerized micelles with compartments. *Curr. Opin. Colloid Interface Sci.* **2003**, *8*, 274−281.

(2) Li, C.; Zhou, H.; Nguyen, S. *217th ACS National Meeting. INOR-460*, Anaheim, Calif., 1999.

(3) Blanazs, A.; Armes, S. P.; Ryan, A. J. Self-assembled block copolymer aggregates: from micelles to vesicles and their biological applications. *Macromol. Rapid Commun.* **2009**, *30*, 267−277.

(4) Moughton, A. O.; Hillmyer, M. A.; Lodge, T. P. Multicompartment block polymer micelles. *Macromolecules* **2012**, *45*, 2−19.

(5) Skrabania, K.; Berlepsch, H.; Böttcher, C.; Laschewsky, A. Synthesis of Ternary, Hydrophilic−Lipophilic−Fluorophilic Block Copolymers by Consecutive RAFT Polymerizations and Their Self-Assembly into Multicompartment Micelles. *Macromolecules* **2010**, *43*, 271−281.

(6) Skrabania, K.; Laschewsky, A.; Berlepsch, H.; Böttcher, C. Synthesis and micellar self-assembly of ternary hydrophilic−lipophilic−fluorophilic block copolymers with a linear PEO chain. *Langmuir* **2009**, *25*, 7594−7601.

(7) Li, Z.; Hillmyer, M. A.; Lodge, T. P. Morphologies of multicompartment micelles formed by ABC miktoarm star terpolymers. *Langmuir* **2006**, *22*, 9409−9417.

(8) Ahmed, E.; Womble, C. T.; Cho, J.; Dancel-Manning, K.; Rice, W. J.; Jang, S. S.; Weck, M. One-pot synthesis of linear triblock terpolymers and their aqueous self-assembly. *Polym. Chem.* **2021**, *12*, 1967−1974.

(9) Kubowicz, S.; Baussard, J. F.; Lutz, J. F.; Thünemann, A. F.; von Berlepsch, H.; Laschewsky, A. Multicompartment micelles formed by self-assembly of linear ABC triblock copolymers in aqueous medium. *Angew. Chem., Int. Ed.* **2005**, *44*, 5262−5265.

(10) Marsat, J.-N.; Heydenreich, M.; Kleinpeter, E.; Berlepsch, H.; Böttcher, C.; Laschewsky, A. Self-Assembly into Multicompartment Micelles and Selective Solubilization by Hydrophilic−Lipophilic−Fluorophilic Block Copolymers. *Macromolecules* **2011**, *44*, 2092−2105.

(11) Ahmed, E.; Womble, C. T.; Weck, M. Synthesis and Aqueous Self-Assembly of ABCD Bottlebrush Block Copolymers. *Macromolecules* **2020**, *53*, 9018−9025.

(12) Marsat, J.-N.; Stahlhut, F.; Laschewsky, A.; Berlepsch, H.; Böttcher, C. Multicompartment micelles from silicone-based triphilic block copolymers. *Colloid Polym. Sci.* **2013**, *291*, 2561−2567.

(13) Lodge, T. P.; Rasdal, A.; Li, Z.; Hillmyer, M. A. Simultaneous, segregated storage of two agents in a multicompartment micelle. *J. Am. Chem. Soc.* **2005**, *127*, 17608−17609.

(14) Li, Z.; Kesselman, E.; Talmon, Y.; Hillmyer, M. A.; Lodge, T. P. Multicompartment micelles from ABC miktoarm stars in water. *Science* **2004**, *306*, 98−101.

(15) Li, S.; He, J.; Zhang, M.; Wang, H.; Ni, P. Multicompartment morphologies self-assembled from fluorinated ABC triblock terpolymers: the effects of flexible and rigid hydrophobic moieties. *Polym. Chem.* **2016**, *7*, 1773−1781.

(16) Nayanathara, U.; Kermaniyan, S. S.; Such, G. K. Multicompartment Polymeric Nanocarriers for Biomedical Applications. *Macromol. Rapid Commun.* **2020**, *41*, No. 2000298.

(17) Liu, H.; Zhao, Y.; Dreiss, C. A.; Feng, Y. CO2-switchable multicompartment micelles with segregated corona. *Soft Matter* **2014**, *10*, 6387−6391.

(18) Liu, H.; Guo, Z.; He, S.; Yin, H.; Feng, Y. Synthesis and self-assembly of ABC linear triblock copolymers to target CO2-responsive multicompartment micelles. *RSC Adv.* **2016**, *6*, 86728−86735.

(19) Wong, C. K.; Chen, F.; Walther, A.; Stenzel, M. H. Bioactive patchy nanoparticles with compartmentalized cargoes for simultaneous and trackable delivery. *Angew. Chem., Int. Ed.* **2019**, *131*, 7413−7418.

(20) Akhter, D. T.; Simpson, J. D.; Fletcher, N. L.; Houston, Z. H.; Fuchs, A. V.; Bell, C. A.; Thurecht, K. J. Oral Delivery of Multicompartment Nanomedicines for Colorectal Cancer Therapeutics: Combining Loco-Regional Delivery with Cell-Target Specificity. *Adv. Ther.* **2020**, *3*, No. 1900171.

(21) Rinkenauer, A. C.; Schallon, A.; Günther, U.; Wagner, M.; Betthausen, E.; Schubert, U. S.; Schacher, F. H. A paradigm change: efficient transfection of human leukemia cells by stimuli-responsive multicompartment micelles. *ACS Nano* **2013**, *7*, 9621−9631.

(22) Synatschke, C. V.; Nomoto, T.; Cabral, H.; Förtsch, M.; Toh, K.; Matsumoto, Y.; Miyazaki, K.; Hanisch, A.; Schacher, F. H.; Kishimura, A.; Nishiyama, N.; Müller, A. H. E.; Kataoka, K. Multicompartment micelles with adjustable poly (ethylene glycol) shell for efficient in vivo photodynamic therapy. *ACS Nano* **2014**, *8*, 1161−1172.

(23) Nomoto, T.; Fukushima, S.; Kumagai, M.; Machitani, K.; Matsumoto, Y.; Oba, M.; Miyata, K.; Osada, K.; Nishiyama, N.; Kataoka, K. Three-layered polyplex micelle as a multifunctional nanocarrier platform for light-induced systemic gene transfer. *Nat. Commun.* **2014**, *5*, 3545.

(24) Nghiem, T.-L.; Coban, D.; Tjaberings, S.; Gröschel, A. H. Recent Advances in the Synthesis and Application of Polymer Compartments for Catalysis. *Polymer* **2020**, *12*, 2190.

(25) Womble, C. T.; Kuepfert, M.; Weck, M. Multicompartment Polymeric Nanoreactors for Non-Orthogonal Cascade Catalysis. *Macromol. Rapid Commun.* **2019**, *40*, No. 1800580.

(26) Qu, P.; Cleveland, J. W.; Ahmed, E.; Liu, F.; Dubrawski, S.; Jones, C. W.; Weck, M. Compartmentalisation of molecular catalysts for nonorthogonal tandem catalysis. *Chem. Soc. Rev.* **2022**, *51*, 57−70.

(27) Qu, P.; Kuepfert, M.; Ahmed, E.; Liu, F.; Weck, M. Cross-Linked Polymeric Micelles as Catalytic Nanoreactors. *Eur. J. Inorg. Chem.* **2021**, *2021*, 1420−1427.

(28) Rzayev, J. Molecular Bottlebrushes: New Opportunities in Nanomaterials Fabrication. *ACS Macro Lett.* **2012**, *1*, 1146−1149.

(29) Lin, T.-P.; Chang, A. B.; Luo, S.-X.; Chen, H.-Y.; Lee, B.; Grubbs, R. H. Effects of grafting density on block polymer self-assembly: From linear to bottlebrush. *ACS Nano* **2017**, *11*, 11632−11641.

(30) Cheng, L.-C.; Gadelrab, K. R.; Kawamoto, K.; Yager, K. G.; Johnson, J. A.; Alexander-Katz, A.; Ross, C. A. Templated self-assembly of a PS-branch-PDMS bottlebrush copolymer. *Nano Lett.* **2018**, *18*, 4360−4369.

(31) Ma, H.; Kim, K. T. Self-assembly of bottlebrush block copolymers into triply periodic nanostructures in a dilute solution. *Macromolecules* **2020**, *53*, 711−718.

(32) Sheiko, S. S.; Sumerlin, B. S.; Matyjaszewski, K. Cylindrical molecular brushes: Synthesis, characterization, and properties. *Prog. Polym. Sci.* **2008**, *33*, 759−785.

(33) Xie, G.; Martinez, M. R.; Olszewski, M.; Sheiko, S. S.; Matyjaszewski, K. Molecular bottlebrushes as novel materials. *Biomacromolecules* **2018**, *20*, 27−54.

(34) Choinopoulos, I. Grubbs' and Schrock's catalysts, ring opening metathesis polymerization and molecular brushes—synthesis, characterization, properties and applications. *Polymer* **2019**, *11*, 298.

(35) Radzinski, S. C.; Foster, J. C.; Scannelli, S. J.; Weaver, J. R.; Arrington, K. J.; Matson, J. B. Tapered bottlebrush polymers: Cone-shaped nanostructures by sequential addition of macromonomers. *ACS Macro Lett.* **2017**, *6*, 1175−1179.

(36) Walsh, D. J.; Dutta, S.; Sing, C. E.; Guironnet, D. Engineering of molecular geometry in bottlebrush polymers. *Macromolecules* **2019**, *52*, 4847−4857.

(37) Walsh, D. J.; Guironnet, D. Macromolecules with programmable shape, size, and chemistry. *Proc. Natl. Acad. Sci. U. S. A.* **2019**, *116*, 1538−1542.

(38) Fenyves, R.; Schmutz, M.; Horner, I. J.; Bright, F. V.; Rzayev, J. Aqueous self-assembly of giant bottlebrush block copolymer surfactants as shape-tunable building blocks. *J. Am. Chem. Soc.* **2014**, *136*, 7762−7770.

(39) List, B. Proline-catalyzed asymmetric reactions. *Tetrahedron* **2002**, *58*, 5573−5590.

(40) Movassaghi, M.; Jacobsen, E. N. The simplest "enzyme". *Science* **2002**, *298*, 1904−1905.

(41) Bahmanyar, S.; Houk, K. The origin of stereoselectivity in proline-catalyzed intramolecular aldol reactions. *J. Am. Chem. Soc.* **2001**, *123*, 12911−12912.

(42) List, B.; Lerner, R. A.; Barbas, C. F. Proline-catalyzed direct asymmetric aldol reactions. *J. Am. Chem. Soc.* **2000**, *122*, 2395−2396.

(43) Suri, J. T.; Mitsumori, S.; Albertshofer, K.; Tanaka, F.; Barbas, C. F. Dihydroxyacetone variants in the organocatalytic construction of carbohydrates: mimicking tagatose and fuculose aldolases. *J. Org. Chem.* **2006**, *71*, 3822−3828.

(44) Sakthivel, K.; Notz, W.; Bui, T.; Barbas, C. F. Amino acid catalyzed direct asymmetric aldol reactions: a bioorganic approach to catalytic asymmetric carbon−carbon bond-forming reactions. *J. Am. Chem. Soc.* **2001**, *123*, 5260−5267.

(45) Pihko, P. M.; Laurikainen, K. M.; Usano, A.; Nyberg, A. I.; Kaavi, J. A. Effect of additives on the proline-catalyzed ketone−aldehyde aldol reactions. *Tetrahedron* **2006**, *62*, 317−328.

(46) Ibrahem, I.; Córdova, A. Amino acid catalyzed direct enantioselective formation of carbohydrates: one-step de novo synthesis of ketoses. *Tetrahedron Lett.* **2005**, *46*, 3363−3367.

(47) Torii, H.; Nakadai, M.; Ishihara, K.; Saito, S.; Yamamoto, H. Asymmetric direct aldol reaction assisted by water and a proline-derived tetrazole catalyst. *Angew. Chem., Int. Ed.* **2004**, *43*, 1983−1986.

(48) Aratake, S.; Itoh, T.; Okano, T.; Nagae, N.; Sumiya, T.; Shoji, M.; Hayashi, Y. Highly diastereo-and enantioselective direct aldol reactions of aldehydes and ketones catalyzed by siloxyproline in the presence of water. *Chem. — Eur. J.* **2007**, *13*, 10246−10256.

(49) Gruttadauria, M.; Giacalone, F.; Mossuto Marculescu, A.; Lo Meo, P.; Riela, S.; Noto, R. Hydrophobically Directed Aldol Reactions: Polystyrene-Supported L-Proline as a Recyclable Catalyst for Direct Asymmetric Aldol Reactions in the Presence of Water. *Eur. J. Org. Chem.* **2007**, *2007*, 4688.

(50) Chimni, S. S.; Mahajan, D.; Babu, V. S. Protonated chiral prolinamide catalyzed enantioselective direct aldol reaction in water. *Tetrahedron Lett.* **2005**, *46*, 5617−5619.

(51) Sheldon, R. A. The E factor 25 years on: the rise of green chemistry and sustainability. *Green Chem.* **2017**, *19*, 18−43.

(52) Breslow, R. Hydrophobic effects on simple organic reactions in water. *Acc. Chem. Res.* **1991**, *24*, 159−164.

(53) Manabe, K.; Mori, Y.; Wakabayashi, T.; Nagayama, S.; Kobayashi, S. Organic synthesis inside particles in water: lewis acid− surfactant-combined catalysts for organic reactions in water using colloidal dispersions as reaction media. *J. Am. Chem. Soc.* **2000**, *122*, 7202−7207.

(54) Hailes, H. C. Reaction solvent selection: the potential of water as a solvent for organic transformations. *Org. Process Res. Dev.* **2007**, *11*, 114−120.

(55) Sheldon, R. A. Green solvents for sustainable organic synthesis: state of the art. *Green Chem.* **2005**, *7*, 267−278.

(56) Lu, A.; Smart, T. P.; Epps, T. H., III; Longbottom, D. A.; O'Reilly, R. K. l-Proline functionalized polymers prepared by RAFT polymerization and their assemblies as supported organocatalysts. *Macromolecules* **2011**, *44*, 7233−7241.

(57) Lipshutz, B. H.; Ghorai, S. Organocatalysis in water at room temperature with in-flask catalyst recycling. *Org. Lett.* **2012**, *14*, 422−425.

(58) Kuepfert, M.; Ahmed, E.; Weck, M. Self-assembled thermoresponsive molecular brushes as nanoreactors for asymmetric aldol addition in water. *Macromolecules* **2021**, *54*, 3845−3853.

(59) Lu, A.; Cotanda, P.; Patterson, J. P.; Longbottom, D. A.; O'Reilly, R. K. Aldol reactions catalyzed by L-proline functionalized polymeric nanoreactors in water. *Chem. Commun.* **2012**, *48*, 9699−9701.

(60) Zayas, H. A.; Lu, A.; Valade, D.; Amir, F.; Jia, Z.; O'Reilly, R. K.; Monteiro, M. J. Thermoresponsive polymer-supported L-proline micelle catalysts for the direct asymmetric aldol reaction in water. *ACS Macro Lett.* **2013**, *2*, 327−331.

(61) Lu, A.; Moatsou, D.; Longbottom, D. A.; O'Reilly, R. K. Tuning the catalytic activity of L-proline functionalized hydrophobic nanogel particles in water. *Chem. Sci.* **2013**, *4*, 965−969.

(62) Liu, C.; Hillmyer, M. A.; Lodge, T. P. Evolution of multicompartment micelles to mixed corona micelles using solvent mixtures. *Langmuir* **2008**, *24*, 12001−12009.

(63) Smith, D.; Pentzer, E. B.; Nguyen, S. T. Bioactive and therapeutic ROMP polymers. *J. Macromol. Sci., Polym. Rev.* **2007**, *47*, 419−459.

(64) Choi, T. L.; Grubbs, R. H. Controlled Living Ring-Opening-Metathesis Polymerization by a Fast-Initiating Ruthenium Catalyst. *Angew. Chem., Int. Ed.* **2003**, *42*, 1743−1746.

(65) Bielawski, C. W.; Grubbs, R. H. Living ring-opening metathesis polymerization. *Prog. Polym. Sci.* **2007**, *32*, 1−29.

(66) Kuepfert, M.; Cohen, A. E.; Cullen, O.; Weck, M. Shell Cross-Linked Micelles as Nanoreactors for Enantioselective Three-Step Tandem Catalysis. *Chem. − Eur. J.* **2018**, *24*, 18648−18652.

(67) Whitfield, R.; Anastasaki, A.; Nikolaou, V.; Jones, G. R.; Engelis, N. G.; Discekici, E. H.; Fleischmann, C.; Willenbacher, J.; Hawker, C. J.; Haddleton, D. M. Universal conditions for the controlled polymerization of acrylates, methacrylates, and styrene via Cu (0)-RDRP. *J. Am. Chem. Soc.* **2017**, *139*, 1003−1010.

(68) Bates, C. M.; Chang, A. B.; Momčilović, N. a.; Jones, S. C.; Grubbs, R. H. ABA triblock brush polymers: Synthesis, self-assembly, conductivity, and rheological properties. *Macromolecules* **2015**, *48*, 4967−4973.

(69) Gerle, M.; Fischer, K.; Roos, S.; Müller, A. H.; Schmidt, M.; Sheiko, S. S.; Prokhorova, S.; Möller, M. Main chain conformation and anomalous elution behavior of cylindrical brushes as revealed by GPC/MALLS, light scattering, and SFM. *Macromolecules* **1999**, *32*, 2629−2637.

(70) Gröschel, A. H.; Schacher, F. H.; Schmalz, H.; Borisov, O. V.; Zhulina, E. B.; Walther, A.; Müller, A. H. Precise hierarchical self-assembly of multicompartment micelles. *Nat. Commun.* **2012**, *3*, 710.

(71) Callaway, C. P.; Hendrickson, K.; Bond, N.; Lee, S. M.; Sood, P.; Jang, S. S. Molecular Modeling Approach to Determine the Flory-Huggins Interaction Parameter for Polymer Miscibility Analysis. *Chem. Phys. Chem.* **2018**, *19*, 1655−1664.

(72) Cho, J.; Choi, J. I.; Jang, S. S. Structural Transformation of a Multicompartment Micelle Induced by Photo-Switchable Spiropyran−Merocyanine Transition: Dissipative Particle Dynamics Simulation Approach. *J. Phys. Chem. B* **2022**, *126*, 4401−4410.

(73) He, T.; Li, K.; Wu, M.-Y.; Wu, M.-B.; Wang, N.; Pu, L.; Yu, X.-Q. Water promoted enantioselective aldol Reaction by proline-cholesterol and-diosgenin based amphiphilic organocatalysts. *Tetrahedron* **2013**, *69*, 5136−5143.